Forward Neuromusculoskeletal Dynamics With Continuous Muscle Wrapping

Iram Muñoz-Pepi, Nadia Garcia-Hernandez, and Vicente Parra-Vega

***Abstract*—This letter investigates an explicit biomechanical framework to solve forward neuromusculoskeletal models (NMSMs), which includes muscle-tendon activation and contraction dynamics, musculoskeletal coupling, and multibody dynamics. The study addresses a novel muscle-wrapping method to compute the shortest muscle-tendon path using a $\mathcal{C}^1$ geodesic-based approach subject to tangency constraints, yielding an analytical formulation of muscle-tendon length and velocity, and a closed-form moment arm Jacobian matrix. A simple but representative upper limb NMSM was simulated under two conditions: (I) with no external wrench applied and (II) with a time-varying external wrench applied on the wrist simulating an interaction with a robot. For condition (I), our proposal was compared with OpenSim. Results from simulation under condition (I) show that the waveform of the analyzed parameters is similar to that obtained in OpenSim. Still, the proposed method yields overall improved results due to the analytical computation of muscle-tendon velocity and moment arm Jacobian matrix. Regarding the results under condition II, they show the reliability of the proposed modular NMSM framework to simulate human-robot interaction dynamics. Henceforth, our continuous wrapping-based NMSM proposal contributes as a baseline to model and study more representative forward NMSMs to assess human movement, including interaction with robots.**

***Index Terms*—Geodesics, modeling and simulating humans, muscle wrapping, neuromusculoskeletal systems, tendon/wire mechanism.**

I. Introduction

MODELING and simulation of human neuromusculoskeletal systems are of great interest to assess muscle activation and joint forces for given human movements from neural commands or vice versa [1]. In particular, a forward dynamic NMSM can provide muscle-to-joint forces after neural excitation and its causal skeletal movement. NMSMs overcome the disadvantages of in-vivo methods that are subject-specific and, therefore, challenging to scale; however, its validity remains commensurable to how tractable and precise the model is. A NMSM consists of four interconnected subsystems; see Fig. 1. In subsystem 1), muscle-tendon activation dynamics are commanded by neural excitation generated in the Central Nervous System (CNS). In subsystem 2), the muscle-tendon force generation is computed from a non-linear model based on muscle contraction and tendon elastic properties (i.e., the Hill-type model [2]). Consequently, the calculated muscle-tendon force requires estimating muscle length and velocity, whose values depend on how realistic muscle-tendon paths are modeled. Subsystem 3) includes the musculoskeletal coupling model to calculate muscle-tendon length and velocity considering wrapping and non-wrapping paths over bone surfaces. In this subsystem, the modeling of the muscle moment arms is considered. In subsystem 4), the multibody Lagrangian dynamics are commanded by the joint torques (which are produced by muscle forces), either in forward or feedback configuration. Modeling and simulating all four subsystems is very complex since it involves highly non-linear dynamic couplings requiring a multidisciplinary approach. Indeed, alternative and powerful computational tools, such as OpenSim [1], have been developed, implementing some numerical approximations in its latest releases. For instance, it remains to be seen how to compute the analytical muscle-tendon velocity and the moment arm Jacobian matrix, let alone $\mathcal{C}^1$ wrapping paths. Though there also exists powerful methods proposed by the robotics community, they have addressed 2) – 4) as three disjoint problems under different assumptions, namely wrapping in cable-driven robots without involving Hill model [3], biomechanical dynamics neglecting muscle-tendon [4] and constrained and task-level control problems, [5]. Few works have addressed the four interconnected

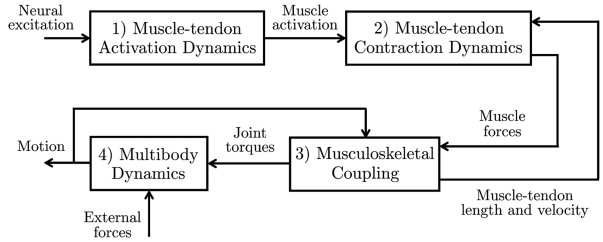

Fig. 1. Forward NMSM subsystem interconnections, where input is the neural excitation, and output is the skeletal motion.

Manuscript received 15 March 2023; accepted 12 July 2023. Date of publication 31 July 2023; date of current version 10 August 2023. This letter was recommended for publication by Associate Editor L. Peternel and Editor A. Bera upon evaluation of the reviewers' comments. The work of Iram Muñoz-Pepi was supported by the National Council of Humanities, Science and Technology of Mexico (CONAHCYT) with the scholarship under Grant CVU#861816. *(Corresponding author: Nadia Garcia-Hernandez.)*

Iram Muñoz-Pepi and Vicente Parra-Vega are with the Department of Robotics and Advanced Manufacturing, Research Center for Advanced Studies (CINVESTAV), Ramos Arizpe 25900, Mexico (e-mail: iram.munoz@cinvestav.mx; vparra@cinvestav.mx).

Nadia Garcia-Hernandez is with the Department of Robotics and Advanced Manufacturing, Research Center for Advanced Studies (CINVESTAV), Ramos Arizpe 25900, Mexico, also with the Rehab Technologies Lab, Italian Institute of Technology, 16163 Genova, Italy, and also with the National Council of Humanities, Science and Technology of Mexico (CONAHCYT), Mexico city 03940, Mexico (e-mail: nadia.garcia@iit.it, nadia.garcia@cinvestav.mx).

This letter has supplementary downloadable material available at https://doi.org/10.1109/LRA.2023.3300277, provided by the authors.

Digital Object Identifier 10.1109/LRA.2023.3300277

subsystems of a NMSM; under restrictive assumptions, [4] neglects well-posed wrapping, [6] does not consider neural excitation, [7] does not compute analytically the moment arm Jacobian matrix, nor muscle-tendon velocity [4].

Modeling muscle-tendon paths requires an accurate description of the muscles wrapping state to calculate reliable muscle forces. This can be challenging because some muscles cannot be represented by a single straight line but by a curved path over surfaces [8]. Sophisticated muscle-tendon wrapping methods [9], [10] use geodesic theory to compute the shortest path over parametric surfaces, which remains untested for NMSM. A drawback in these methods is that they cannot ensure $\mathcal{C}^1$ continuity since they neglect the geodesic's tangency constraints, leading to a solution sensitive to initial guess.

This letter investigates an explicit biomechanical four-step framework to solve forward NMSMs. Unlike previous works, our NMSM approach includes a $\mathcal{C}^1$ continuous and well-posed muscle wrapping algorithm based on tangency constraints, which facilitates the analytical formulation of muscle-tendon length and velocity required to estimate muscle forces and a closed-form moment arm Jacobian matrix. Illustrative forward dynamic simulations for a simple but representative upper limb model are presented for two conditions: (I) with no external wrench applied and (II) with a time-varying external wrench applied on the wrist due to the interaction with a robot. In addition, for condition (I), results were compared versus those obtained with OpenSim.

II. Background

This section presents a brief review of relevant literature to establish the context of the proposal: modular analytical modeling of a forward dynamic NMSM (see Fig. 1). The modular architecture of the proposed framework is in line with that used in other open-source software for biomechanical simulations, such as OpenSim [1] and Artisynth [11].

The excitation of neural and muscular tissue, called neural excitation, acts through activation dynamics to generate an internal muscle tissue state (i.e., muscle activation) [2]. Complete human movement studies address neural excitations through optimal control [12] or feedback control [13]. However, we limit the scope of the study to feed-forward neural excitation signals to assess the contribution of our proposal. On the other hand, the muscle activation dynamics have been modeled using a typical equation of restitution that represents the solution of a nonlinear first-order differential equation [2], [12]. It relates the rate of change of muscle activation (i.e., the concentration of calcium ions within the muscle) to the muscle excitation (i.e., the firing of motor units). This activation energizes the cross-bridges through muscle contraction dynamics, and muscle force is developed. Several muscle contraction models [14], [15], [16] are derived after the 85 years old Hill's model [17], which uses force-length-velocity properties of muscle fibers and the elastic properties of tendons. Notice that smooth muscle-tendon lengths and velocities produce smooth forces; hence continuous muscle-tendon path models are essential for realistic skeletal movement.

Advanced methods for muscle-tendon path computation concatenate straight lines with geodesic segments [10]; however, they may generate non-continuous paths because their formulation only guarantees continuity at some configurations. Compared to Artisynth software, Opensim integrates the obstacle-set method [18] to compute exact muscle-tendon wrapping path length over spheres and cylinders. Yet, it also includes a hybrid approximation approach for ellipsoids based on [19]. However, the analytical solution of the essential muscle-tendon velocity must still be addressed.

Synthesis of the musculoskeletal dynamics stands, in fact, for two associated problems relating to the nonlinear differential equation that models Lagrange dynamics: the unforced Lagrange dynamics and the forcing generalized input. The unforced Lagrange dynamics assume the NMSM's body segment inertial parameters to be lumped parameters; moreover, these can be estimated using regression models [20] or by scaling generic musculoskeletal models in OpenSim [1]. Biomechanical studies provide the foundations of robot-like Lagrangian dynamics assuming rigid bodies [20]; thus, its structural properties comply with the typical Euler-Lagrangian robot dynamics [21]. On the other hand, the forcing input of Lagrange dynamics is computed from the muscle contraction forces and the moment arms, provided by a muscle-tendon wrapping formulation. Regarding this problem, the computation of the moment arms has been addressed, avoiding calculating muscle-tendon velocity [22]. Thus, it stands nowadays as a bottleneck for either off-line or attempting online applications leading to compromising accuracy, precision, and latency [23]. Furthermore, several studies have introduced polynomials to estimate muscle-tendon lengths, velocities, and moment arms for solving high-dimensional problems, such as predictive simulations through optimal control [24], [25]. They not only require twice continuously differentiable models for second-order gradient-based optimization algorithms but also to reduce the high computational cost [26]. Considering the lack of an analytical method for calculating muscle-tendon lengths, velocities, and moment arms, this letter presents a method for calculating such muscle quantities.

III. Methodology

For completeness, we briefly introduce the underlying formulation for subsystems 1) and 2), while full details are developed for subsystems 3) and 4). The explicit contribution of our proposal, in subsystems 3) and 4), is threefold: it amounts to i) well-posed $\mathcal{C}^1$ wrapping to compute muscle-tendon length and velocity, leading to the ii) moment arm Jacobian matrix formulation, and the iii) multibody musculoskeletal dynamics actuated by Hill forces, elicited from neural excitations.

A. Muscle-Tendon Activation Dynamics: Subsystem 1

The CNS issues the neural excitation $0 \leq e \leq 1$ to drive the following nonlinear first-order differential equation [12] modeling muscle activation a as its state

$$\frac{da}{dt} = \left[\frac{(f+0.5)}{\tau_a\,(0.5+1.5a)} - \frac{(f-0.5)\,(0.5+1.5a)}{\tau_d}\right](e-a) \tag{1}$$

where $f = 0.5\tanh(b(e-a))$ smooths the transition between muscle activation and deactivation, with a smoothing factor $b > 0$, while $\tau_a > 0$ and $\tau_d > 0$ are the muscle activation and deactivation time constants, respectively, for $\tau_a < \tau_d$, [2].

B. Muscle-Tendon Contraction Force: Subsystem 2

The well-known muscle contraction Hill-type model [2], consists of muscle and tendon elements in series (SE). Muscle fibers are represented by an active contractile element (CE) parallel to a passive element (PE). The orientation α of muscle fibers with respect to tendon stands for the pennation angle. Muscle-tendon length l_{MT} depends on muscle length l_M, pennation angle and tendon length l_T as follows

$$l_{MT} = l_T + l_M\cos(\alpha), \tag{2}$$

where l_M is related to the optimal fiber length l_M^0 and pennation angle α_0 by $l_M\sin(\alpha) = l_M^0\sin(\alpha_0)$. For a given maximum isometric force F_M^0, the total muscle force F_M becomes

$$F_M = F_M^0\left[af_{act}\left(\tilde{l}_M\right)f_v\left(\tilde{v}_M\right) + f_{pas}\left(\tilde{l}_M\right)\right], \tag{3}$$

where $\tilde{l}_M$ is the normalized muscle length to l_M^0, with $\tilde{v}_M$ its muscle fiber velocity normalized to the maximal velocity $v_M^{\max}$, and f_v, f_{act}, and f_{pas}, are the muscle force-velocity, and the active and passive muscle force-length curves, respectively, in accordance to [12]. Now, since F_M depends on active F_{CE} and passive F_{PE} forces, then the force F_s transmitted from the muscle to the tendon depends on the pennation angle $F_s = [F_{CE} + F_{PE}]\cos\alpha = F_M\cos\alpha$, which relates to the tendon force F_T by $F_T = F_M^0 f_t(\tilde{l}_T)$, for $\tilde{l}_T$ the normalized tendon length to tendon slack length l_T^s and f_t the tendon force-length curve [12]. Now, assuming an elastic tendon and a negligible muscle's mass, the forces are at equilibrium, then $F_s = F_T$, which is solved for F_M.

C. Musculoskeletal Coupling: Subsystem 3

1) Muscle-Tendon Wrapping: When a muscle-tendon is in contact with a wrapping surface, the muscle-tendon path segment is composed of two straight lines, anchored at origin Q^{i-1} and insertion P^{i+1} points, connected through a curve-line (geodesic) wrapping the bony joint, see Fig. 2. The straight-line segment is given by $l^i = \| P^i - Q^{i-1} \|$ whereas the curved-line segment is represented by an arc length (s) parametrized curve, also known as unit speed curve [27], $\mathbf{r}(s) = \mathbf{r}(u(s), v(s)) : \mathbb{R}^2 \mapsto \mathbb{R}^3$, for $s_{P^i} \leq s \leq s_{Q^i}$, where surface coordinates (u, v), and their derivatives w.r.t. arc length (u', v'), determine the geodesic direction, and the arc length s. The total muscle-tendon length can be therefore obtained as

$$l_{MT} = l^i + s^i + l^{i+1} \tag{4}$$

where

$$s^i(w) = \int_{w_{P^i}}^{w_{Q^i}} \| \bar{\mathbf{r}}(w) \| \, dw, \tag{5}$$

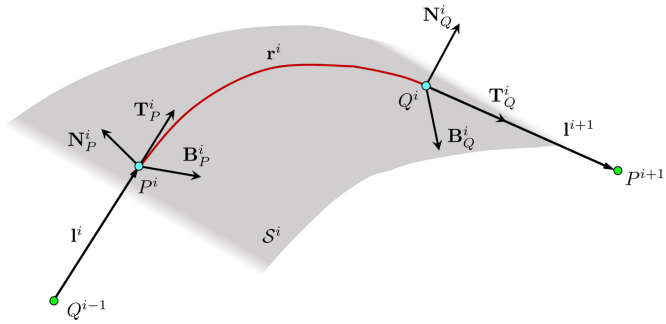

Fig. 2. A well-posed wrapping path is obtained when tangent vectors $\mathbf{T}_P^i$ and $\mathbf{T}_Q^i$ are aligned with vectors $\mathbf{l}^i$ and $\mathbf{l}^{i+1}$, respectively. Here, the muscle is anchored to the origin Q^{i-1} and insertion P^{i+1} points, gray surface depicts the bony surface and geodesic (red) represents the curved wrapping segment.

notation $(\dot{\cdot})$ denotes the differentiation w.r.t. w; $\mathbf{r}(w_{P^i}) = {}^{(i)}P^i$ and $\mathbf{r}(w_{Q^i}) = {}^{(i)}Q^i$ from (5). To compute the time derivative of (4) we first find the derivative of the straight-line segment length l^i as

$$\dot{l}^i = \mathbf{l}^i \cdot \left({}^{(0)}\dot{P}^i - {}^{(0)}\dot{Q}^{i-1}\right), \quad \text{for } \mathbf{l}^i = \frac{P^i - Q^{i-1}}{\| P^i - Q^{i-1} \|}$$

and for curved-line segment (5) one obtains

$$\dot{s}(w) = \frac{dw}{dt}\left(\left\|\bar{\mathbf{r}}(w_{Q^i})\right\| - \left\|\bar{\mathbf{r}}(w_{P^i})\right\|\right) \tag{6}$$

Enforcing minimum l_{MT} length, i.e. $\nabla_w l_{MT}(w) = 0$ leads to

$$\frac{P^i - Q^{i-1}}{\| P^i - Q^{i-1} \|} = \frac{\bar{\mathbf{r}}(w_{P^i})}{\left\|\bar{\mathbf{r}}(w_{P^i})\right\|}, \tag{7}$$

$$\frac{P^{i+1} - Q^i}{\| P^{i+1} - Q^i \|} = \frac{\bar{\mathbf{r}}(w_{Q^i})}{\left\|\bar{\mathbf{r}}(w_{Q^i})\right\|}. \tag{8}$$

Substituting the time derivative of ${}^{(i)}P^i$ and ${}^{(i)}Q^i$ into the time derivatives of (7) and (8), respectively, the following expressions are obtained

$$\mathbf{l}^i \cdot {}^{(i)}\dot{P}^i = \frac{dw}{dt}\left\|\bar{\mathbf{r}}(w_{P^i})\right\|, \tag{9}$$

$$\mathbf{l}^{i+1} \cdot {}^{(i)}\dot{Q}^{i+1} = \frac{dw}{dt}\left\|\bar{\mathbf{r}}(w_{Q^i})\right\|. \tag{10}$$

Then, using (9) and (10), (6) can be rewritten as follows $\dot{s}^i = \left(\mathbf{l}^{i+1} \cdot {}^{(i)}\dot{Q}^i\right) - \left(\mathbf{l}^i \cdot {}^{(i)}\dot{P}^i\right)$ where ${}^{(0)}\dot{P}^i = {}^{(0)}\dot{R}^i + {}^{(i)}\dot{P}^i$, and ${}^{(0)}\dot{Q}^i = {}^{(0)}\dot{R}^i + {}^{(i)}\dot{Q}^i$, for the position ${}^{(0)}R^i$ and velocity ${}^{(0)}\dot{R}^i$ of surface's $\mathcal{S}^i$ origin w.r.t Σ_0. Thus, the muscle-tendon velocity arises as follows

$$\dot{l}_{MT} = \mathbf{l}^{i+1} \cdot {}^{(0)}\dot{P}^{i+1} - \mathbf{l}^i \cdot {}^{(0)}\dot{Q}^{i-1} + \mathbf{l}^i \cdot {}^{(0)}\dot{R}^i - \mathbf{l}^{i+1} \cdot {}^{(0)}\dot{R}^i \tag{11}$$

where $\dot{P}^{i+1}$ and $\dot{Q}^{i-1}$ are the velocities of the insertion and origin points, respectively.

To enforce $\mathcal{C}^1$ continuity at connection points P^i and Q^i, let the tangency error function be modeled as a constraint by using

(7) and (8) as follows

$$\mathbf{f}(\mathbf{x}^i) = \begin{bmatrix} \mathbf{l}^i - \mathbf{T}_{P^i} \\ \mathbf{l}^{i+1} - \mathbf{T}_{Q^i} \end{bmatrix} = 0 \tag{12}$$

where $\mathbf{x}^i = [\, u_{P^i} \quad v_{P^i} \quad u'_{P^i} \quad v'_{P^i} \quad s^i \,]^T$. To solve (12) for geodesic parameters $\mathbf{x}^i$ we propose in this letter the so-called Smooth Geodesic Wrapping (SGW) method using the Broyden's method [28] and a free-derivative line search algorithm [29].

2) Moment Arm Jacobian Matrix: The linear operator matrix $\mathbf{R} \in \mathbb{R}^{n\times m}$ maps generalized coordinate velocities $\dot{\mathbf{q}} \in \mathbb{R}^n$ to muscle-tendon velocities $\dot{\mathbf{l}}_{MT} \in \mathbb{R}^m$ as

$$\dot{\mathbf{l}}_{MT} = \frac{d}{dt}\mathbf{l}_{MT} = \frac{\partial \mathbf{l}_{MT}}{\partial \mathbf{q}} \frac{d\mathbf{q}}{dt} = \mathbf{R}\dot{\mathbf{q}},$$

where r_{ij} is an entry of $\mathbf{R}$ and the moment arm of the jth muscle-tendon unit with respect to the ith joint. Let $\mathbf{R}_w$ denote the moment arm matrix when wrapping exists, which can be obtained by solving (11),

$$\begin{aligned} \mathbf{R}_w = {} & \mathbf{l}^{(i+1)^T} \begin{bmatrix} -{}^0\mathbf{E}_{\lambda_P} \left[{}^{(\lambda_P)}\boldsymbol{r}_{P^{i+1}} \times \right] & {}^0\mathbf{E}_{\lambda_P} \end{bmatrix} {}^{(\lambda_P)}\mathbf{J}_{\lambda_P} \\ & - \mathbf{l}^{(i)^T} \begin{bmatrix} -{}^0\mathbf{E}_{\lambda_Q} \left[{}^{(\lambda_Q)}\boldsymbol{r}_{Q^{i-1}} \times \right] & {}^0\mathbf{E}_{\lambda_Q} \end{bmatrix} {}^{(\lambda_Q)}\mathbf{J}_{\lambda_Q} \\ & + \mathbf{l}^{(i)^T} \begin{bmatrix} -{}^0\mathbf{E}_{\lambda_S} \left[{}^{(\lambda_S)}\boldsymbol{r}_{S^i} \times \right] & {}^0\mathbf{E}_{\lambda_S} \end{bmatrix} {}^{(\lambda_S)}\mathbf{J}_{\lambda_S} \\ & - \mathbf{l}^{(i+1)^T} \begin{bmatrix} -{}^0\mathbf{E}_{\lambda_S} \left[{}^{(\lambda_S)}\boldsymbol{r}_{S^i} \times \right] & {}^0\mathbf{E}_{\lambda_S} \end{bmatrix} {}^{(\lambda_S)}\mathbf{J}_{\lambda_S} \end{aligned} \tag{13}$$

where ${}^i\mathbf{E}_j$ is the rotation matrix of Σ_j expressed in Σ_i coordinates, ${}^i\boldsymbol{r}_j$ is a position vector following the latter convention, $\mathbf{J} \in \mathbb{R}^{6\times n}$ is the geometric Jacobian matrix, and λ_P, λ_Q, λ_S represent the parent frames of P^{i+1}, Q^{i-1}, S^i, respectively. Now, when the muscle-tendon is not in contact with a wrapping surface, the total path is represented by a single straight-line segment, then, using (11) and given that velocity ${}^{(0)}\dot{R}^i = 0$, a non-wrapping moment arm Jacobian matrix $\mathbf{R}_{nw}$ can be expressed as

$$\begin{aligned} \mathbf{R}_{nw} = {} & \mathbf{l}^T \begin{bmatrix} -{}^0\mathbf{E}_{\lambda_P} \left[{}^{(\lambda_P)}\boldsymbol{r}_{P^{i+1}} \times \right] & {}^0\mathbf{E}_{\lambda_P} \end{bmatrix} {}^{(\lambda_P)}\mathbf{J}_{\lambda_P} - \\ & \mathbf{l}^T \begin{bmatrix} -{}^0\mathbf{E}_{\lambda_Q} \left[{}^{(\lambda_Q)}\boldsymbol{r}_{Q^{i-1}} \times \right] & {}^0\mathbf{E}_{\lambda_Q} \end{bmatrix} {}^{(\lambda_Q)}\mathbf{J}_{\lambda_Q} \end{aligned} \tag{14}$$

D. Multibody Dynamics: Subsystem 4

The equations of motion of an n-DoF musculoskeletal human body system subject to external forces and actuated by m muscle-tendon units, commanded by muscle excitation e, can be obtained with the classical Lagrangian formalism of robot-like systems

$$\mathbf{H}(\mathbf{q})\ddot{\mathbf{q}} + \mathbf{C}(\mathbf{q}, \dot{\mathbf{q}})\dot{\mathbf{q}} + \mathbf{G}(\mathbf{q}) = -\mathbf{R}^T\mathbf{f}_m + \mathbf{J}^T\mathbf{f}_e \tag{15}$$

where $\mathbf{q} \in \mathbb{R}^n$ denotes the generalized joint positions; $\mathbf{H}(\mathbf{q}) \in \mathbb{R}^{n\times n}$ models the generalized mass inertia, $\mathbf{C}(\mathbf{q}, \dot{\mathbf{q}}) \in \mathbb{R}^n$ represents the Coriolis matrix, where the quadratic terms of vector $\mathbf{C}(\mathbf{q}, \dot{\mathbf{q}})\dot{\mathbf{q}}$ represents centrifugal forces and the cross product terms the centripetal forces; $\mathbf{G} \in \mathbb{R}^n$ is the vector of gravity terms; external wrench $\mathbf{f}_e \in \mathbb{R}^6$ represents non-endogenous forces either from a disturbance or payload, or while interacting with another system, such as a robot, and $\mathbf{f}_m \in \mathbb{R}^m$ stands for muscle forces whose negative sign indicates contraction forces. Finally, notice that

$$\boldsymbol{\tau} = -\mathbf{R}^T\mathbf{f}_m$$

can be interpreted as the forcing (control) input that commands the motion solution of the musculoskeletal system denoted in (15), that when connected to muscle excitation signal (1), the force $\mathbf{f}_m$ controls the forward NMSM dynamic motion, as described in Fig. 1.

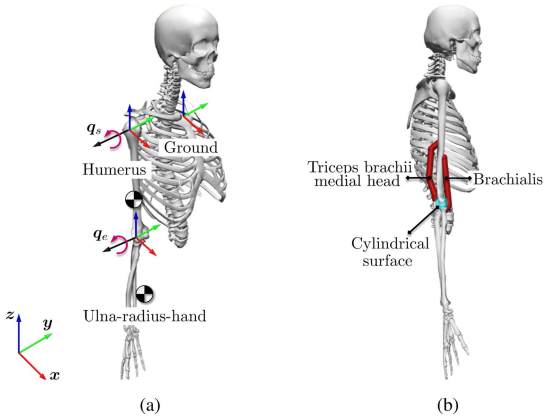

Fig. 3. 3D render (a) of the musculoskeletal upper limb model used, (b) driven by two muscle-tendon units actuating the elbow joint.

E. Musculoskeletal Model

A modified version of the 2 DoF "arm26" OpenSim upper limb model (displayed in Fig. 3), [30], was modeled. The model consists of an underactuated shoulder joint but actuated elbow joint throughout triceps medial head and brachialis muscles. The kinematic chain consists of three connecting bodies: the ground, the humerus, and the forearm (ulna-radius-hand complex). The shoulder joint q_s connects the humerus to the ground and the elbow joint q_e connects the forearm to the humerus. The muscle wrapping surface, a cylinder, is fixed to the humerus such that the triceps medial head and brachialis could wrap over the back and front of the cylindrical surface (see Fig. 3(b)), respectively, within certain ranges of motion of the elbow. Kinematic and inertial parameters were not modified from the original model. The range of motion of each DoF was limited by introducing a viscoelastic torsional spring τ_{pas}, arising from passive joint ligaments stiffness, capsules, and surrounding soft tissue, [31], given by

$$\tau_{pas_i} = \begin{cases} \gamma + k_2\left(q_{i_{\min}} - q_i\right)^2, & \text{if } q_{i_{\min}} < q_i \\ \gamma, & \text{if } q_{i_{\min}} \le q_i < q_{i_{\max}} \\ \gamma - k_2\left(q_i - q_{i_{\max}}\right)^2, & \text{if } q_i \le q_{i_{\max}} \end{cases}$$

where $\gamma = -k_1 q_i - b_p \dot{q}_i$, $q_{i_{\min}}$ and $q_{i_{\max}}$ are the minimum and maximum ith joint limits, k_1, k_2 and b_p are stiffness and damping coefficients, respectively, as given in Table I.

TABLE I
JOINT PASSIVE PROPERTIES USED FOR THE MUSCULOSKELETAL MODEL

Joint	k_1 Nm/rad	k_2 Nm/rad^2	b_p Nm s/rad	q_{min} rad	q_{max} rad
Shoulder	1.0	10000	1.0	$-\pi/2$	π
Elbow	1.0	10000	1.0	0	$13\pi/18$

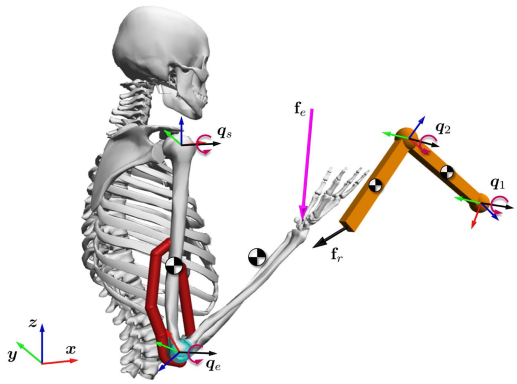

Fig. 4. Three-dimensional musculoskeletal upper limb model subject to forward dynamic robot unilateral interaction. A wrench $\mathbf{f}_r$ is generated by the robot and applied to the wrist of the upper limb model.

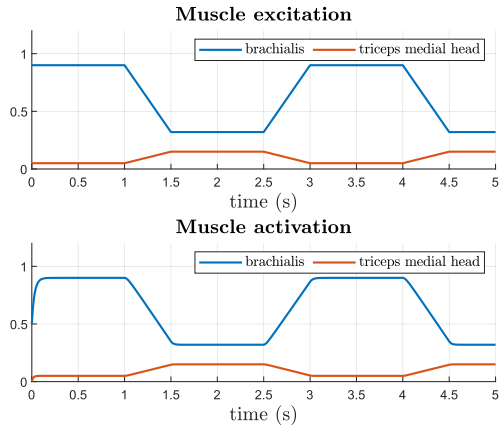

Fig. 5. Normalized forward muscle excitation signals (top) and resultant muscular activation (bottom) for brachialis (blue line) and triceps medial head (orange line).

F. Dynamic Simulations

The forward upper limb NMSM was simulated under two conditions: (I) without applying an external wrench and (II) with a time-varying external wrench ($\mathbf{f}_e$) applied on the wrist due to the interaction with a robot. The simulation under condition I was performed using the proposed framework presented in Section III and using OpenSim (Muscle Analysis Tool).

The simulation under condition II was achieved by modeling the unilateral interaction between a 2 DoF dynamic robot's end-effector and the wrist of the upper limb NMSM, as shown in Fig. 4. The interaction occurs as follows: the motion generated by the robot is under a PD controller regulating a sinusoidal reference path for the first joint (q_1) and a set point reference for the second joint (q_2). The robot torques ($\boldsymbol{\tau}_r$) are transformed into a wrench $\mathbf{f}_r$ at its end-effector frame, i.e. $\mathbf{f}_r = \mathbf{J}_{ee}^{-T}\boldsymbol{\tau}_r$, then transformed firstly to the ground reference frame and then to the upper limb wrist reference frame. Finally, $\mathbf{f}_e$ was mapped through the Jacobian $\mathbf{J}^T$, as in (15). The mass, inertia, length, and center of mass considered for the robot's links were: $(m_1, m_2) = (0.3, 0.21)$Kg, $(I_1, I_2) = (\text{diag}[0.0250, 0.0251, 0.0001], \text{diag}[0.0086, 0.0086, 0.0001])$ Kg $\cdot$ m^2, $(l_1, l_2) = (1.0, 0.7)$m, and $(l_{c1}, l_{c2}) = (-0.5, -0.35)$m. The joint viscous friction coefficients considered were $(b_1, b_2) = (3, 3)\text{N} \cdot \text{s} \cdot \text{rad}^{-1}$.

Brachialis (a_b) and triceps medial head muscle (a_t) activations were evaluated with $\tau_a = 0.015$ s, $\tau_d = 0.060$ s, and $b = 0.1$. Moreover, the tendon strain due to maximum isometric force was set to 0.049. In all simulations, the forward excitation signal shown in Fig. 5 was used. It was designed using a trapezoidal waveform (through Fourier series expansion) with a rise and fall time of 0.5 s, width of 1 s, and period of 3 s. In addition, the upper limb initial conditions were set to $(q_s(0), q_e(0)) = (0, 0.349066)$rad, $(\dot{q}_s(0), \dot{q}_e(0)) = (0, 0)\text{rad} \cdot \text{s}^{-1}$, for muscle activations $(a_b(0), a_t(0)) = (0.5, 0.001)$, and for muscle normalized lengths $(\tilde{l}_b(0), \tilde{l}_t(0)) = (1.01, 0.64)$. The specific requirements for the simulations performed with the proposed framework and OpenSim API are described next.

1) Proposed Framework: The simulator was programmed in MATLAB R2020b running fixed-step Runge-Kutta (ode4) integrator with a step-size of 10 ms. The cylindrical wrapping surface was modeled as $\mathbf{r}(u, v) = \begin{bmatrix} r\cos u & r\sin u & v \end{bmatrix}^T$ with radius $r = 0.016$ m.

2) OpenSim (Muscle Analysis Tool): The simulation was build using the C++ OpenSim API (on Microsoft Visual Studio Community v17.6.0 IDE), the Runge-Kutta-Merson integrator was used through the Manager::IntegratorMethod class and the minimum and maximum integration step sizes were set to 10 ms. The muscle model, viscoelastic passive generalized forces, and muscle excitation signals were implemented using the OpenSim::DeGrooteFregly2016Muscle, OpenSim::Force and OpenSim::Controller classes, respectively. Additionally, the computation of mechanical work and power was implemented in MATLAB using a fixed-step Runge-Kutta (ode4) integrator with a step-size of 10 ms.

IV. RESULTS AND DISCUSSION

The muscle excitation input signals shown in Fig. 5 caused the brachialis and triceps medial head to change from a non-wrapping to a wrapping state, or vice versa. To visualize in all graphs when this happened, shadow areas with different colors were used. Blue and orange shadow areas indicate when the brachialis and triceps medial head muscles were in a wrapping state, respectively. No color was used to indicate when the muscles were in a non-wrapping state. The coding in MATLAB used in this letter and videos are available at the following link: https://github.com/irammunoz/NMSM_Forward_Dynamics.

A. Results for Condition I: No External Wrench Applied

Muscle-tendon length and velocity of the brachialis and triceps medial head are plotted in Fig. 6. Almost overlapped

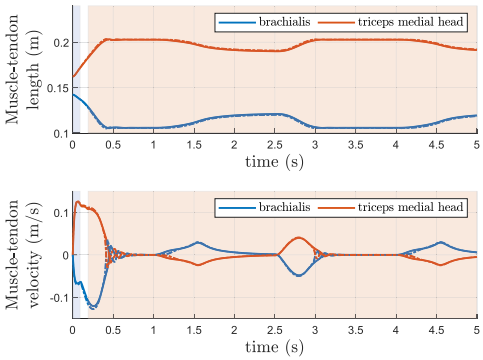

Fig. 6. Muscle-tendon length (top) and velocity (bottom) for brachialis (blue line) and triceps medial head (orange line) are depicted for the proposed framework (solid lines) and OpenSim Muscle Analysis Tool (dashed lines).

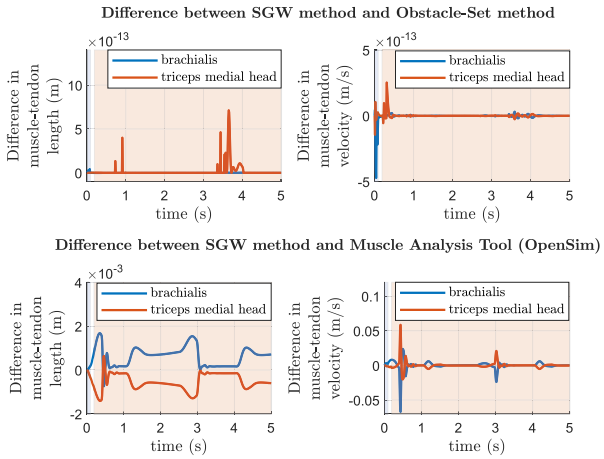

Fig. 7. Differences in muscle-tendon length and velocity between the proposed method (SGW) and the analytical solution (top plots), and between the SGW and OpenSim method (Muscle Analysis Tool) (bottom plots).

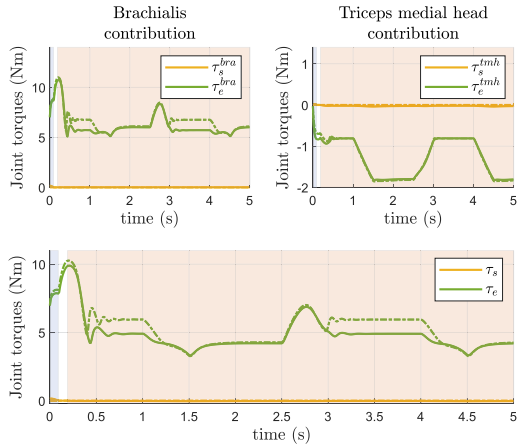

Fig. 8. Joint torques produced by the brachialis (top left) and the triceps medial head (top right), solutions provided by the proposed framework (solid lines), and OpenSim Muscle Analysis Tool (dashed lines). The bottom plot shows the total torques produced by the muscle-tendon units.

results in muscle-tendon lengths were obtained with both methods, but with slight differences of a maximum of 1.7 mm for the brachialis and 1.4 mm for the triceps medial head, see top graph in Fig. 6. With respect to the muscle-tendon velocity, the proposed method yields a smoother profile than those obtained with OpenSim, especially when approaching values close to zero (around $t = 0.5,\ 1.1,\ 3.0,\ 4.1$ s). This was expected since OpenSim calculates muscle-tendon velocity using an approximation method (implemented in GeometryPath::computeLengtheningSpeed class) that calculates the total muscular velocity by adding the velocity of each via point that connects the straight lines over the wrapping path. The maximum differences encountered in muscle-tendon velocity are 67 mm/s for the brachialis and 58.5 mm/s for the triceps medial head (Fig. 6 bottom graph).

While OpenSim provides an analytical solution to the muscle-tendon length around a cylinder (and some other geometries) using the Obstacle-Set method [18], the velocity is approximated using a $\mathcal{C}^0$ via point method that introduces not only deviation but it fails to guarantee continuity. The Obstacle-Set method and its analytical expression for muscle-tendon velocity were simulated in MATLAB to investigate the difference between the proposed method (SGW) and OpenSim (Muscle Analysis Tool). For this simulation, the results show negligible differences in muscle-tendon length and velocity, see Fig. 7 (top plots). However, evident differences are observed between the proposed and OpenSim method as a consequence of the muscle-tendon velocity approximation made by OpenSim, this is because the wrapping path is state-dependent, (see bottom plots of Fig. 7). Likewise, muscle-tendon velocity affects quantities such as joint torques, generalized coordinates, generalized velocities, and energy, so deviations are introduced in all these variables.

Joint torques generated over time by the activation of the brachialis and triceps medial head muscles are shown in the top plots of Fig. 8 and the net joint torques are shown in the bottom plot of Fig. 8. Notice that a considerable difference is observed between the joint torques calculated with the proposed and the Opensim method. This difference is more evident in the joint torque generated by the brachialis muscle (Fig. 8, top left plot). Such torque profiles differ not only in magnitude but also in frequency due to the less smooth muscle-tendon velocity behavior generated with OpenSim (Fig. 6, bottom plot). The effect of the muscle-tendon velocity behavior obtained with each method is also evident in the generalized velocities (Fig. 9, bottom plot), but with less impact in the generalized positions (Fig. 9, top plot) since the integration step filters out inconsistencies in generalized velocities.

The top plot of Fig. 10 depicts the wrist operational position, showing differences up to 6.9 mm in x-axis, 0.64 mm in y-axis, and 18.8 mm in z-axis between simulation approaches. Notice that such apparently small deviations may lead to an unacceptable performance in many high-precision motion tasks, let alone for human-robot interaction tasks where such errors may wrongly indicate that a non-contact condition is achieved when there is an ongoing penetration. The computation of power and work is shown at the bottom plots of Fig. 10, where it can be appreciated that larger values were obtained with the OpenSim method. Notably, smaller work (1.21 W) and power (16.27 J) are obtained with our proposal.

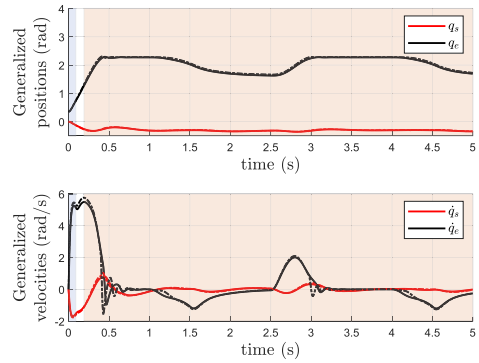

Fig. 9. Joint positions and velocities show maximum differences (1.80e-2 rd, 3.10e-1 rd/s) for q_s and (7.16e-2 rd, 2.93 rd/s) for q_e by comparing the proposed framework (solid lines) and OpenSim Muscle Analysis Tool (dashed lines).

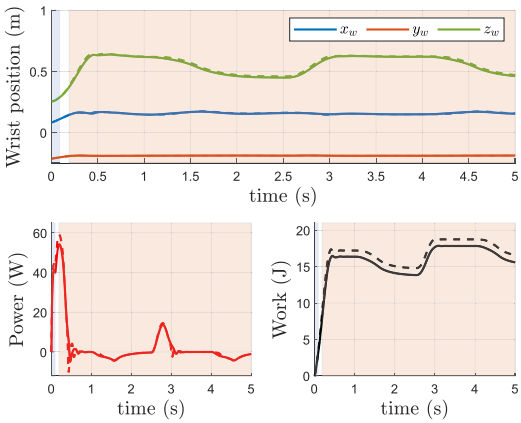

Fig. 10. Difference in operational wrist coordinates (top), mechanical power (bottom left) and work (bottom right) computed using our proposed framework (solid line) and OpenSim Muscle Analysis Tool (dashed line).

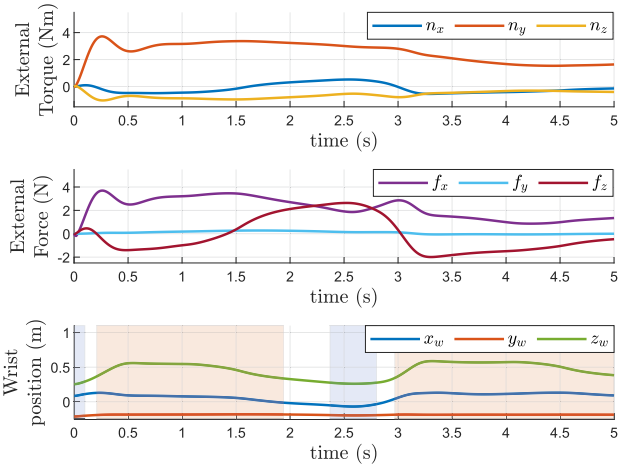

Fig. 11. NMSM motion subject to external torques n (top) and forces f (middle) computed while interacting with inertial robot. The resultant wrist's operational coordinates (bottom) are smooth, despite the endogenous f_e and the commutation between wrapping and non-wrapping.

B. Results for Condition II: External Interaction Wrench

The moment and force components of wrench $\mathbf{f}_e$ are shown in the top and middle plots of Fig. 11, while the wrist spatial position is shown in the bottom plot. Remarkable differences can be seen in the wrist position when comparing it with that obtained under condition I (Fig. 10, top plot). The maximum differences were 229 mm on x-axis, 8.3 mm on y-axis, and 272.9 mm on z-axis, which correspond to similar force magnitudes, i.e. larger in x- and z-axes from larger interaction f_x, f_z, as well as the moment n_y. In addition, the resulting configuration of the upper limb due to the externally applied wrench causes the brachialis and triceps medial head muscles to transition more than once between a wrapping and non-wrapping state (see shaded areas in Fig. 11, bottom plot). Note that smooth transitions between those states were always preserved due to the overall proposed analytical formulation.

V. Conclusion and Future Work

This manuscript presents a general wrapped-based NMSM multibody procedure to solve the forward dynamics problem of NMSM commanded by neuro excitation that issue muscle activation. The proposed framework generates analytical expressions of muscle length and velocity, and therefore a closed-form expression of the moment arm Jacobian matrix. The numerical effectiveness of the developed framework was examined by simulating a simplified upper limb NMSM OpenSim model under neuro-excitation forward command and comparing the results with those obtained from a simulation performed in OpenSim. In addition, endogenous unilateral interaction wrench, which arise from the interaction of the NMSM with a dynamic robot, was modeled and simulated. Results showed the reliability of the proposed modular framework to solve forward dynamical NMSMs, including when external contact forces are applied. Results differed noticeably when muscle velocities were approximated using via points (OpenSim method), thus highlighting the importance of considering exact and smooth muscle wrapping path and velocity computations. The latter claim has the clear message that simplifications or approximation of wrapping are highly numerically sensitive, leading to a less accurate description of muscle-tendon physiology, and therefore movement.

In accordance with the limited but representative simulation study, the proposed framework shows the following advantages: 1) computation of continuous muscle-tendon paths using a $\mathcal{C}^1$ geodesic-based wrapping approach subject to tangency constraints, 2) analytical formulation of muscle-tendon length and velocity needed to compute muscle forces and a closed-form moment arm Jacobian matrix that is used to map muscle forces into joint torques, and 3) the modular architecture enables studying more complex forward NMSMs.

A potential limitation of the present study is the validation of the proposed framework with a simple NMSM, which precludes to conclude its potential of scalability for complex NMSM. We forecast that implementation of a complex case, aimed at a compromise of accuracy and latency, regression models, such as polynomials [32], can be characterized from the SGW method to estimate muscle-related quantities while maintaining low error and alleviating the computational bottleneck. In this aim, there

remains a rigorous comparison study against regression models to strictly oversee spatial accuracy and precision with respect to latency on a representative simulation. Moreover, as we are using Featherstone's dynamics algorithms [21], complex joint types can be considered by adding the joint-specific code, however, the joint motion based on user-specified data [33] is not supported (a feature found in some OpenSim NMSM models). Another issue is the need to introduce robustness to the initialization for the SGW method, which can be explored by introducing virtual control to steer geodesics to a consistent solution space. Finally, the presented framework is also limited by the assumption of a massless wire muscle model (which considers an infinitesimal muscle-tendon width), and therefore a study considering surface wrapping with an infinitesimal pressure point, including lumped parameter friction, remains a future extension.

The long-term goal of this study is triple, firstly to determine the inverse dynamics for interconnection of interaction tasks, meaning the extension of Lagrangian dynamics subject to force constraint due to the closed-kinematic chain, then to solve the inverse dynamics of each NMSM subsystem to finally compute the neural excitation command that produces a given skeletal trajectory. This long-sought objective can be devised by solving the inverse dynamics of neural excitation command, which remains an open subject in the literature. Also, we aim to derive faster numerical methods to attempt online NMSM movement and human-robot interaction assessments. We believe such goals are feasible given our proposal.

REFERENCES

[1] A. Seth et al., "OpenSim: Simulating musculoskeletal dynamics and neuromuscular control to study human and animal movement," *PLoS Comput. Biol.*, vol. 14, no. 7, 2018, Art. no. e1006223.

[2] F. E. Zajac, "Muscle and tendon: Properties, models, scaling, and application to biomechanics and motor control," *Crit. Rev. Biomed. Eng.*, vol. 17, no. 4, pp. 359–411, 1989.

[3] M. C. Lei, "Dynamics of cable driven parallel manipulator allowing cable wrapping over rigid link," in *Proc. IEEE/ASME Int. Conf. Adv. Intell. Mechatronics*, 2020, pp. 215–221.

[4] J. Penner and S. Leyendecker, "A discrete mechanics approach for musculoskeletal simulations with muscle wrapping," *Multibody Syst. Dyn.*, vol. 56, no. 3, pp. 267–287, 2022.

[5] V. De Sapio, O. Khatib, and S. Delp, "Least action principles and their application to constrained and task-level problems in robotics and biomechanics," *Multibody Syst. Dyn.*, vol. 19, no. 3, pp. 303–322, 2008.

[6] A. Ruggiero and A. Sicilia, "A novel explicit analytical multibody approach for the analysis of upper limb dynamics and joint reactions calculation considering muscle wrapping," *Appl. Sci.*, vol. 10, no. 21, 2020, Art. no. 7760.

[7] F. Gao, M. Damsgaard, J. Rasmussen, and S. T. Christensen, "Computational method for muscle-path representation in musculoskeletal models," *Biol. Cybern.*, vol. 87, no. 3, pp. 199–210, 2002.

[8] E. Desailly et al., "The convex wrapping algorithm: A method for identifying muscle paths using the underlying bone mesh," *J. Biomech.*, vol. 43, no. 13, pp. 2601–2607, 2010.

[9] A. Scholz et al., "Improved muscle wrapping algorithms using explicit path-error Jacobians," in *Computational Kinematics*. Berlin, Germany: Springer, 2014, pp. 395–403.

[10] A. Scholz et al., "A fast multi-obstacle muscle wrapping method using natural geodesic variations," *Multibody Syst. Dyn.*, vol. 36, no. 2, pp. 195–219, 2016.

[11] J. Lloyd, I. Stavness, and S. Fels, *ArtiSynth: A Fast Interactive Biomechanical Modeling Toolkit Combining Multibody and Finite Element Simulation*. Berlin, Germany: Springer, 2012.

[12] F. De Groote, A. L. Kinney, A. V. Rao, and B. J. Fregly, "Evaluation of direct collocation optimal control problem formulations for solving the muscle redundancy problem," *Ann. Biomed. Eng.*, vol. 44, no. 10, pp. 2922–2936, 2016.

[13] D. G. Thelen and F. C. Anderson, "Using computed muscle control to generate forward dynamic simulations of human walking from experimental data," *J. Biomech.*, vol. 39, no. 6, pp. 1107–1115, 2006.

[14] L. M. Schutte, M. M. Rodgers, F. E. Zajac, and R. M. Glaser, "Improving the efficacy of electrical stimulation-induced leg cycle ergometry: An analysis based on a dynamic musculoskeletal model," *IEEE Trans. Rehabil. Eng.*, vol. 1, no. 2, pp. 109–125, Jun. 1993.

[15] D. G. Thelen, "Adjustment of muscle mechanics model parameters to simulate dynamic contractions in older adults," *J. Biomech. Eng.*, vol. 125, no. 1, pp. 70–77, 2003.

[16] M. Millard, T. Uchida, A. Seth, and S. L. Delp, "Flexing computational muscle: Modeling and simulation of musculotendon dynamics," *J. Biomech. Eng.*, vol. 135, no. 2, 2013, Art. no. 021005.

[17] A. V. Hill, "The heat of shortening and the dynamic constants of muscle," *Proc. Roy. Soc. London. Ser. B. - Biol. Sci.*, vol. 126, no. 843, pp. 136–195, 1938.

[18] B. A. Garner and M. G. Pandy, "The obstacle-set method for representing muscle paths in musculoskeletal models," *Comput. Methods Biomech. Biomed. Eng.*, vol. 3, no. 1, pp. 1–30, 2000.

[19] F. C. T. Van der Helm, "The shoulder mechanism: A dynamical approach," Ph.D. dissertation, Dept. Mech. Maritime Mater. Eng., Delft Univ. Technol., Delft, The Netherland, 1991.

[20] D. A. Winter, *Biomechanics and Motor Control of Human Movement*, 4th ed. Hoboken, NJ, USA: Wiley, 2009.

[21] R. Featherstone, *Rigid Body Dynamics Algorithms*, 1st ed. New York, NY, USA: Springer, 2014.

[22] M. A. Sherman, A. Seth, and S. L. Delp, "What is a moment arm? Calculating muscle effectiveness in biomechanical models using generalized coordinates," in *Proc. ASME Des. Eng. Tech. Conf.*, 2013, Art. no. V07BT10A052.

[23] M. G. Carmichael and D. Liu, "Towards using musculoskeletal models for intelligent control of physically assistive robots," in *Proc. IEEE Annu. Int. Conf. Eng. Med. Biol. Soc.*, 2011, pp. 8162–8165.

[24] A. Falisse et al., "Algorithmic differentiation improves the computational efficiency of opensim-based trajectory optimization of human movement," *PLoS One*, vol. 14, no. 10, 2019, Art. no. e0217730.

[25] N. Haralabidis et al., "Modifications to the net knee moments lead to the greatest improvements in accelerative sprinting performance: A predictive simulation study," *Sci. Rep.*, vol. 12, no. 1, 2022, Art. no. 15908.

[26] A. Falisse et al., "Rapid predictive simulations with complex musculoskeletal models suggest that diverse healthy and pathological human gaits can emerge from similar control strategies," *J. Roy. Soc. Interface*, vol. 16, no. 157, 2019, Art. no. 20190402.

[27] D. J. Struik, *Lectures on Classical Differential Geometry*. New York, NY, USA: Dover, 1988.

[28] C. G. Broyden, "A class of methods for solving nonlinear simultaneous equations," *Math. Computation*, vol. 19, pp. 577–593, 1965.

[29] D.-H. Li and M. Fukushima, "A derivative-free line search and global convergence of Broyden-like method for nonlinear equations," *Optim. Methods Softw.*, vol. 13, no. 3, pp. 181–201, 2000.

[30] K. R. Holzbaur, W. M. Murray, and S. L. Delp, "A model of the upper extremity for simulating musculoskeletal surgery and analyzing neuromuscular control," *Ann. Biomed. Eng.*, vol. 33, no. 6, pp. 829–840, 2005.

[31] G. T. Yamaguchi, *Models of the Skeletal System*. Boston, MA, USA: Springer, 2001.

[32] A. Sobinov et al., "Approximating complex musculoskeletal biomechanics using multidimensional autogenerating polynomials," *PLoS Comput. Biol.*, vol. 16, no. 12, 2020, Art. no. e1008350.

[33] A. Seth, M. Sherman, P. Eastman, and S. Delp, "Minimal formulation of joint motion for biomechanisms," *Nonlinear Dyn.*, vol. 62, no. 1, pp. 291–303, 2010.

Open Access funding provided by 'Istituto Italiano di Tecnologia' within the CRUI CARE Agreement